ORIGINAL ARTICLE

Detection and quantification of focal uptake in head and neck tumours: ^{18}F-FDG PET/MR versus PET/CT

Arthur Varoquaux · Olivier Rager · Antoine Poncet · Bénédicte M. A. Delattre ·
Osman Ratib · Christoph D. Becker · Pavel Dulguerov · Nicolas Dulguerov · Habib Zaidi ·
Minerva Becker

Abstract

Purpose Our objectives were to assess the quality of PET images and coregistered anatomic images obtained with PET/MR, to evaluate the detection of focal uptake and SUV, and to compare these findings with those of PET/CT in patients with head and neck tumours.

Methods The study group comprised 32 consecutive patients with malignant head and neck tumours who underwent whole-body ^{18}F-FDG PET/MR and PET/CT. PET images were reconstructed using the attenuation correction sequence for PET/MR and CT for PET/CT. Two experienced observers evaluated the anonymized data. They evaluated image and fusion quality, lesion conspicuity, anatomic location, number and size of categorized (benign versus assumed malignant) lesions with focal uptake. Region of interest (ROI) analysis was performed to determine SUVs of lesions and organs for both modalities. Statistical analysis considered data clustering due to multiple lesions per patient.

Results PET/MR coregistration and image fusion was feasible in all patients. The analysis included 66 malignant lesions (tumours, metastatic lymph nodes and distant metastases), 136 benign lesions and 470 organ ROIs. There was no statistically significant difference between PET/MR and PET/CT regarding rating scores for image quality, fusion quality, lesion conspicuity or anatomic location, number of detected lesions and number of patients with and without malignant lesions. A high correlation was observed for SUV$_{mean}$ and SUV$_{max}$ measured on PET/MR and PET/CT for malignant lesions, benign lesions and organs (ρ =0.787 to 0.877, p <0.001). SUV$_{mean}$ and SUV$_{max}$ measured on PET/MR were significantly lower than on PET/CT for malignant tumours, metastatic neck nodes, benign lesions, bone marrow, and liver (p <0.05). The main factor affecting the difference between SUVs in malignant lesions was tumour size (p <0.01).

Conclusion In patients with head and neck tumours, PET/MR showed equivalent performance to PET/CT in terms of qualitative results. Comparison of SUVs revealed an excellent correlation for measurements on both modalities, but under-estimation of SUVs measured on PET/MR as compared to PET/CT.

A. Varoquaux · O. Rager · B. M. A. Delattre · O. Ratib ·
C. D. Becker · H. Zaidi · M. Becker (✉)
Department of Imaging, Divisions of Radiology and Nuclear
Medicine, Geneva University Hospital, Rue Gabrielle
Perret Gentil 4, CH-1211 Geneva 14, Switzerland
e-mail: Minerva.Becker@hcuge.ch

A. Poncet
Center for Clinical Research, Geneva University Hospital, Geneva,
Switzerland

B. M. A. Delattre
Nuclear Medicine Division, Philips Healthcare AG, Gland,
Switzerland

P. Dulguerov · N. Dulguerov
Clinic of Otorhinolaryngology Head and Neck Surgery,
Geneva University Hospital, Geneva, Switzerland

Introduction

Staging and treatment planning of malignant head and neck tumours require endoscopy with biopsy and additional MRI, CT and/or whole-body ^{18}F-FDG PET/CT. Due to its excellent soft-tissue contrast, MRI is widely used as the first-line approach to imaging head and neck tumours [1, 2]. Since the introduction of 3-T scanners and new coil technology, high-resolution MRI of the head and neck area has become possible in clinical routine with improved results for the staging of primary tumours and for the detection of recurrent disease [1, 2]. However, in the staging

of nodal disease, ^{18}F-FDG-PET/CT has been shown to be superior to conventional anatomic MRI sequences [3], and there is general agreement that PET/CT is indicated whenever distant metastases or second synchronous tumours are suspected [3]. Since the diagnostic information of MRI and PET are complementary, combining the two modalities should facilitate tumour detection and staging. The use of MRI instead of CT for attenuation correction also reduces radiation dose, especially in patients undergoing repeat PET studies [4].

Recently introduced PET/MR systems include new technologic features that allow acquisition of MRI and PET data in the same patient during a single examination providing high-quality fusion of MRI and PET images [5–16]. In the so-called simultaneous PET/MR systems, PET inserts are installed inside the bore of the MRI machine [5], whereas in the so-called sequential PET/MR systems the patient is transferred between the MRI and the PET scanner while remaining on the same table support [6, 16].

The purpose of this prospective study was to assess the feasibility of sequential PET/MR and of PET/MR image fusion, and to compare its performance to that of PET/CT with respect to lesion detection, characterization and anatomic localization of focal uptake in patients with malignant head and neck tumours. In addition, our objective was to compare ^{18}F-FDG uptake quantification with PET/MR and PET/CT despite different PET characteristics, data acquisition and processing protocols.

Materials and methods

Study design and patient selection

This prospective clinical study was approved by the institutional ethics committee and was performed in accordance with the guidelines of the Helsinki II declaration. Over a period of 12 months, we included consecutive patients with head and neck tumours in whom MRI of the head and neck and whole-body ^{18}F-FDG PET/CT were clinically indicated and who gave informed consent to participate in the study. Exclusion criteria were standard contraindications for MRI and refusal to participate in the study. None of the patients potentially eligible for the study refused to participate and all patients were able to sustain both examinations. Therefore, 32 consecutive patients (13 women, 19 men; mean age 59 ± 18 years) with known or suspected head and neck tumours underwent a whole-body PET/MR scan followed by a whole-body PET/CT scan. In 13 patients, the indication for imaging was primary staging of head and neck squamous cell carcinoma (12 patients) or lymphoma (1 patient). In 18 patients, the indication was suspected recurrence of head and neck squamous cell carcinoma (17 patients) or rhabdomyosarcoma (1 patient). In one patient, the indication was head and neck

lymph node metastasis from an unknown primary. The proof of diagnosis consisted of histology (endoscopic biopsy or surgical resection), follow-up ≥12 months or a combination of histology and follow-up. Histologic proof with or without follow-up was available for the primary site in 28 patients, for lymph node status in 18 patients, and for the chest and the remainder of the body in 4 patients. Follow-up alone was the proof of diagnosis in 4 patients for the primary site, in 14 patients for lymph node status, and in 28 patients for the remainder of the body, respectively.

Imaging protocol

All patients received a single ^{18}F-FDG injection, followed by a PET/MR scan and a subsequent PET/CT scan. ^{18}F-FDG (373 ± 28 MBq) was injected in the PET/MR system and the time for radiotracer uptake was used for the diagnostic MRI scan of the head and neck and for total body MRI sequences for attenuation correction and anatomic localization. A whole-body PET acquisition was obtained on the PET/MR system, after which the patient was transferred to the PET/CT scanner. This approach did not require additional injection of ^{18}F-FDG.

PET/MR acquisition

All PET/MR scans were performed on a Philips Ingenuity time-of-flight (TF) PET/MR scanner (Philips Healthcare, Cleveland, OH), which is a sequential PET/MR system consisting of a GEMINI TF PET scanner and an Achieva 3-T TX MRI scanner with a common rotating table platform in between [6, 16]. After radiotracer injection, a dedicated MRI scan of the head and neck was performed using a SENSE neurovascular coil. The voxel size of the T1-weighted (TR/TE 683/16) and T2-weighted (TR/TE 3, 528/90) sequences was $0.45\times0.45\times3$ mm, the voxel size of the diffusion-weighted (TR/TE 3,867/260) sequence was $1.3\times1.3\times3$ mm, and the voxel size of the STIR (TR/TE/TI 5,043/80/200) sequence was $0.45\times0.45\times4$ mm. The dedicated head and neck MRI scan (total acquisition time 40 min) was followed by a whole-body Dixon and MRI attenuation correction sequence using a quadrature body coil. The whole-body Dixon sequence acquired after injection of gadoterate meglumine (Dotarem, 0.1 mmol/kg; Guerbet, Aulnay-sous-Bois, France) had the following parameters: flip angle 10°, TE$_1$ 1.1 ms, TE$_2$ 2.0 ms, TR 3.2 ms, 450×354 mm transverse FOV, voxel size $0.85\times0.85\times3$ mm, total acquisition time 2 min 17 s. This sequence [13, 14, 17] provides four datasets (in-phase and opposed-phase gradient echo images, and derived water-only and fat-only images), among which we prefer the water-only images for anatomic localization and PET/MR data fusion because of their excellent anatomic detail and lesion conspicuity. The MRI-based attenuation correction procedure has

recently been described [18]. This fast multistack whole-body MRI sequence called atMR, is acquired in 2 min 29 s. It consists of a 3-D multistack spoiled T1-weighted gradient echo sequence with the following parameters: flip angle 10°, TE 2.3 ms, TR 4.1 ms, smallest water–fat shift, 600 mm transverse FOV with a slab thickness of 120 mm, voxel size $1.9 \times 1.9 \times 6$ mm. After the atMR acquisition, the table was rotated and the PET scan was performed. PET acquisition was started 85 ± 20 min after injection. It included a total of ten bed positions for a total PET acquisition time of 32 min.

PET/CT acquisition

PET/CT data were acquired on a Biograph 64 True Point scanner (Siemens Healthcare, Erlangen, Germany). The CT scan for attenuation correction and diagnostic purposes had the following parameters: 120 kVp, 180 mAs, collimation 24×1.5, pitch 1.2, 1 s per rotation. The slice thickness of the reconstructed CT images was 2 mm and the reconstruction interval was 1.5 mm. No intravenous or oral contrast material was administered. PET data acquisition was started 146.2 ± 20 min after injection of ^{18}F-FDG with a total of eight or nine bed positions resulting in an acquisition time of $24 - 27$ min. The delay between the two PET acquisitions was 61 ± 20 min and the delay between the end of the PET acquisition on the PET/MR machine and the start of the PET acquisition on the PET/CT machine was on average 29 min. This time lag resulted from the necessity to transport the patient from the PET/MR to the PET/CT unit and to place the patient as similarly as possible to the positioning on the PET/MR table.

Image reconstruction

On the PET/MR system, the MR map obtained by three-class segmentation (air, soft-tissue, lungs) of the corresponding atMR sequence was used to correct the PET images for attenuation. A pre-generated template taking into account table and RF coil attenuation was added to the patient attenuation map. The PET images were reconstructed using a 3-D line-of-response (LOR)/TF/blob-based ordered subsets expectation maximization (OSEM) algorithm and standard parameters recommended by the manufacturer (three iterations, 33 subsets, voxel size $4 \times 4 \times 4$ mm).

On the PET/CT scanner, CT-based PET images were reconstructed using an attenuation-weighted, ordered subset-expectation maximization (AWOSEM) iterative reconstruction algorithm (four iterations, eight subsets, voxel size $4 \times 4 \times 5$ mm). Therefore, a similar voxel size was available for comparison of the PET data from the two modalities.

The standardized uptake values (SUV) for all PET data were calculated according to the standard formula [19].

Image evaluation and SUV measurement

Prior to image evaluation, PET/MR and PET/CT DICOM datasets were anonymized. For each PET/MR examination the whole-body PET, the water-only Dixon and the atMR sequences were available for review. For each PET/CT acquisition, the PET and the unenhanced CT images were analysed. In order to make sure that identical anatomic regions with respect to craniocaudal extent were covered by the two examinations, the images of either modality were truncated so as to cover exactly the same anatomic area explored by the two modalities.

Two physicians with 6 and 16 years of experience reading PET and head and neck MR images evaluated all datasets in consensus. They were blinded to clinical, endoscopic and histopathologic results. In a first session, they evaluated all PET/MR images in a predefined random order and 2 weeks later all the PET/CT images in a different predefined order. The aim of having a gap between the two readings, rating the images in different orders and anonymizing the data was to minimize the effect of memory on lesion detection and characterization.

All images were evaluated on a PACS workstation using OsiriX software (OsiriX v. 4.0, 64 bits; Geneva, Switzerland). For PET/MR, all areas of focal uptake were first identified on axial PET images, after which the atMR and water-only Dixon sequences were used for PET/MR image fusion and to identify the anatomic lesions corresponding to focal uptake. In analogy, for PET/CT, focal uptake was first identified on axial PET images, after which the CT data were used for anatomic correlation. The readers equally evaluated maximum intensity projections of PET images and performed 2-D reconstructions in any other plane whenever necessary.

Analysis of PET/MR and PET/CT data included qualitative and quantitative assessment. Using a three-point scale (poor–moderate–good), the two readers evaluated image quality based on the presence of geometric distortion and breathing or swallowing artifacts, and they assessed areas of focal uptake with respect to alignment between PET and anatomic structures, quality of fusion, lesion conspicuity and anatomic location. Lesions with focal uptake were defined as well-circumscribed areas of increased tracer uptake relative to the surrounding structures. The two readers classified areas of focal uptake either as probably malignant or as probably benign based on visual analysis, asymmetry of tracer uptake and taking into consideration the normal distribution of ^{18}F-FDG in the head and neck region. For the differentiation of malignant from benign focal uptake in the head and neck, a SUV threshold of 3 was used. This threshold was chosen in accordance with the literature [20, 21] and based on our clinical experience. Fusion of PET images with anatomic images from the contrast-enhanced Dixon sequence was used for morphologic correlation. The number of lesions was

recorded. Malignant lesions with focal uptake were further categorized as tumour (T), lymph node metastasis (N) or distant metastasis (M) according to UICC/AJCC recommendations [1]. Benign uptake included inflammatory lesions (such as reactive lymph nodes, sialadenitis, oesophagitis, arteriosclerotic plaques), posttraumatic lesions and physiologic uptake (due to muscle activity or brown fat). The two readers tagged all lesions with focal uptake on the computer screen during the blinded evaluations using different symbols for benign and malignant focal uptake. Tagging was done at the level of the size of the largest lesion. After evaluation and tagging by the two readers, a third physician with 8 years experience in head and neck MRI and PET identified all tagged lesions on both modalities and identified those lesions that were detected on one modality but were missed on the other modality. Discrepant readings were recorded. Then the two readers who had initially rated the PET/MR and PET/CT images reevaluated the discrepant readings to determine whether the lesions missed initially on one modality could be detected retrospectively.

SUVs of all tagged areas of focal uptake were then measured using predefined regions of interest (ROIs) for size and shape saved in DICOM format. The measurements were done on anatomically corresponding PET/MR and PET/CT images of the same patient allowing comparison of SUVs at the same level. Predefined ROIs were also used for measuring SUVs of the liver, lungs, spleen, bone, muscle, salivary glands and background. To ensure that ROIs were placed on the anatomic area to be measured, images were reviewed visually slice-by-slice on the computer screen, as reported by previous investigators [22]. For all ROIs, SUV_{mean} and SUV_{max} were measured. Lesion size was additionally measured according to RECIST criteria.

Statistical analysis

Fisher's exact test was used to compare the number of lesions with focal uptake detected by PET/MR and PET/CT. The Wilcoxon signed-ranks test was used to compare the scores obtained with the two modalities for image quality, fusion quality, anatomic location and conspicuity of focal uptake. Spearman's rank correlation coefficient (ρ) was calculated to assess the correlation between SUV measured on PET/MR and those measured on PET/CT [23]. Concordance between the SUVs from PET/MR and PET/CT (SUV_{mean} and SUV_{max}) was determined according to the methods of Bland and Altman [23, 24]. The limits of agreement were derived from logarithmically transformed values to give limits for the ratio of the actual measurements. Linear mixed models with a random effect on patients for non-normally distributed samples of clustered data were used to calculate the relative difference between SUVs from PET/MR and those from PET/CT accounting for clustering due to multiple lesions per

patient [25, 26]. Linear mixed models were also applied to explore the factors influencing SUVs in malignant lesions and the difference between SUVs from PET/MR and those from PET/CT. The explored factors were lesion size, anatomic region (neck versus chest) and lesion type (malignant tumour, metastatic lymph node, distant metastasis).

Statistical analysis was carried out using a freeware program (R version 2.15.1; The R Foundation for Statistical Computing, Boston, MA). Values of $p < 0.05$ were considered statistically significant.

Results

Image quality, fusion quality, lesion conspicuity and anatomic location

PET/MR and PET/CT examinations were successfully performed in all patients. Image quality, fusion quality, conspicuity and anatomic location of focal uptake were good (Fig. 1). There was no statistically significant difference between mean PET/MR and PET/CT rating scores (Table 1) and there was no mismatch in anatomic location between modalities for any of the lesions with focal uptake. Breathing, swallowing and motion had no major impact on image quality in 31 patients and degraded image quality in one patient on both PET/MR and PET/CT scans. Dental fillings and implants impaired image quality on PET/MR scans in two patients (6.25 %) and on PET/CT scans in four patients (12.5 %; Figs. 2 and 3).
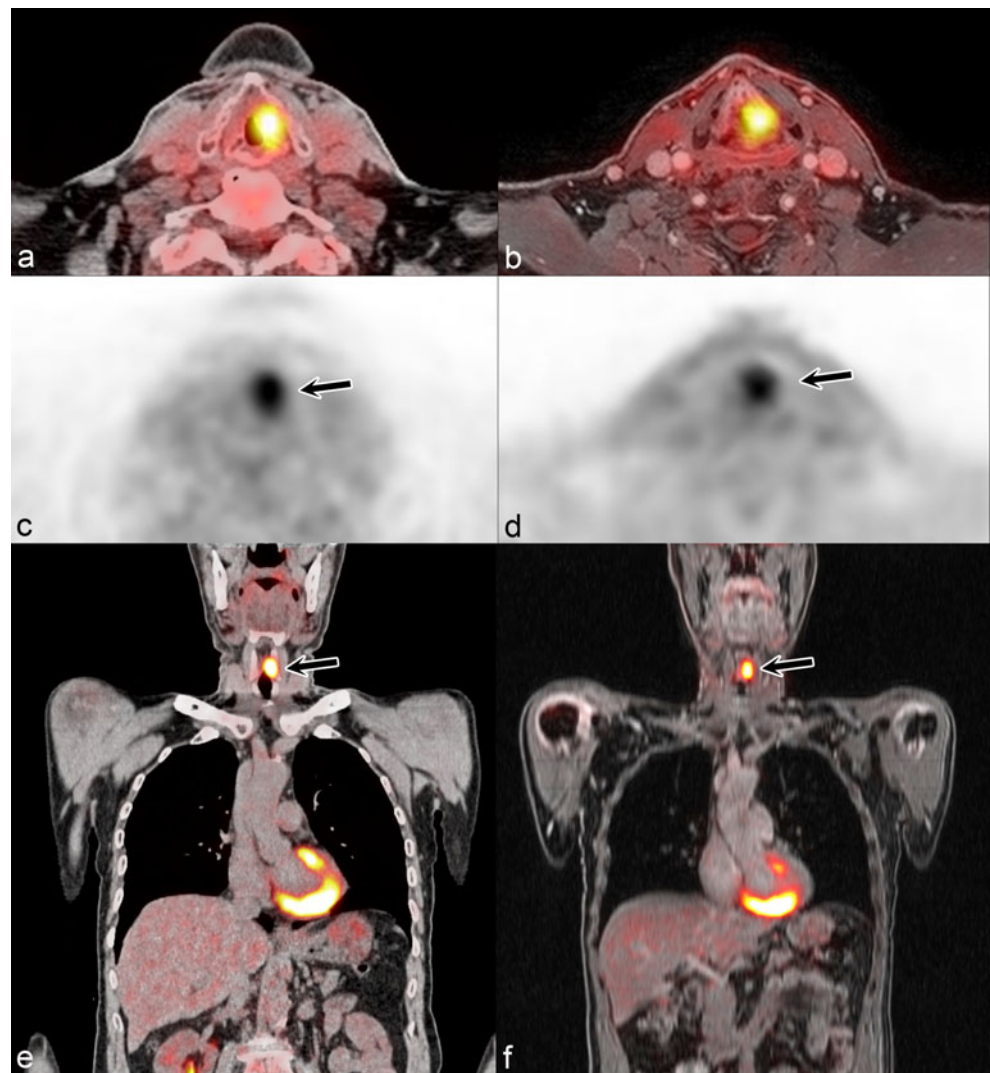
Characteristics of lesions with focal uptake

Based on all available information from the PET/CT and PET/MR datasets, 202 lesions with focal uptake were detected: 66 malignant and 136 benign. The number of lesions with focal uptake varied from zero to 18 lesions per patient with a mean of 7 lesions (benign and malignant) per patient. The anatomic distribution of lesions, presumed lesion type and lesion size are shown in Table 2. The number and characteristics of benign lesions with focal uptake are given in Table 3 and an example is shown in Fig. 4. The majority of benign lesions with focal uptake were of inflammatory origin (104 of 136; Table 2).

Concordant and discordant PET/MR and PET/CT readings

In the patient-based analysis, among the 32 patients included in the study, 28 rated positive for malignant focal uptake on PET/CT were also rated positive on PET/MR and 4 patients rated negative on PET/CT were also rated negative on PET/MR. Based on the final diagnosis, in the lesion-based analysis, there were 32 head and neck tumours (25 patients

Fig. 1 Comparable image quality, fusion quality, lesion conspicuity and anatomic location by PET/CT and PET/MR in a 50-year-old woman with squamous cell carcinoma of the larynx T3N1M0. **a** Fused PET and CT image, **b** fused PET and water-only Dixon MR image, **c** PET image from PET/CT, **d** PET image from PET/MR, **e** fused whole-body PET and CT image, **f** fused PET and water-only Dixon MR image. Distant metastases are absent (*arrows* left glottic tumour)

Table 1 Visual rating scores (1 – 3: poor–moderate–good)

	PET/MR	PET/CT	*p* value
Image quality	2.95±0.25	2.96±0.2	0.18
Fusion quality	2.95±0.29	2.93±0.25	0.62
Lesion conspicuity	2.97±0.22	2.97±0.22	1
Anatomic location	2.95±0.22	2.96±0.2	0.16

p >0.05, nonsignificant

with one head and neck tumour each, 2 patients with two synchronous tumours, and 1 patient with three synchronous tumours), 23 lymph node metastases and 11 distant metastases. Among the malignant lesions with focal uptake identified on PET/CT there were 32 head and neck tumours, 21 lymph node metastases (10 in the neck and 11 in the chest) and 9 distant metastases. On PET/MR, there were 31 malignant

tumours, 22 lymph node metastases (9 in the neck and 13 in the chest) and 9 distant metastases.

Of the total 202 lesions, a discordant rating was present in 8 (3.9 %) in six patients (18.75 %). In six of the discordant ratings, the lesion was either missed on PET/MR or on PET/CT (on PET/MR four lesions seen on PET/CT were missed, and two lesions not seen on PET/CT were detected) and in two the interpretation (benign/malignant) was discordant (Table 4; Fig. 5). The final diagnosis in these eight lesions with a discordant rating was based on histology alone or histology and follow-up in six lesions. In two lesions, the definitive diagnosis was established by follow-up of ≥12 months (Table 4). All eight lesions with discordant ratings had morphologic correlates on CT and on the Dixon sequence and were not caused by artefacts. The lesions missed initially on one modality were identified by the readers retrospectively, the conspicuity of the respective lesion being poor on the modality on which the lesion was initially missed.

Fig. 2 Degraded PET/MR image quality due to dental implants in a 50-year-old woman with recurrent squamous cell carcinoma T3N0M0 of the oral cavity. Moderate PET/MR image quality (score 2) and good PET/CT quality (score 3). Fused image quality, lesion conspicuity and anatomic location were comparable by both modalities (score 3). **a** CT image, **b** water-only Dixon image, **c** fused PET and CT image, **d** fused PET and water-only Dixon MR image, **e** PET image from PET/CT, **f** PET image from PET/MR. Note the comparable visualization and anatomic localization of the tumour (*long arrows*) along the right horizontal branch of the mandible (*short arrows*, dental artefact)
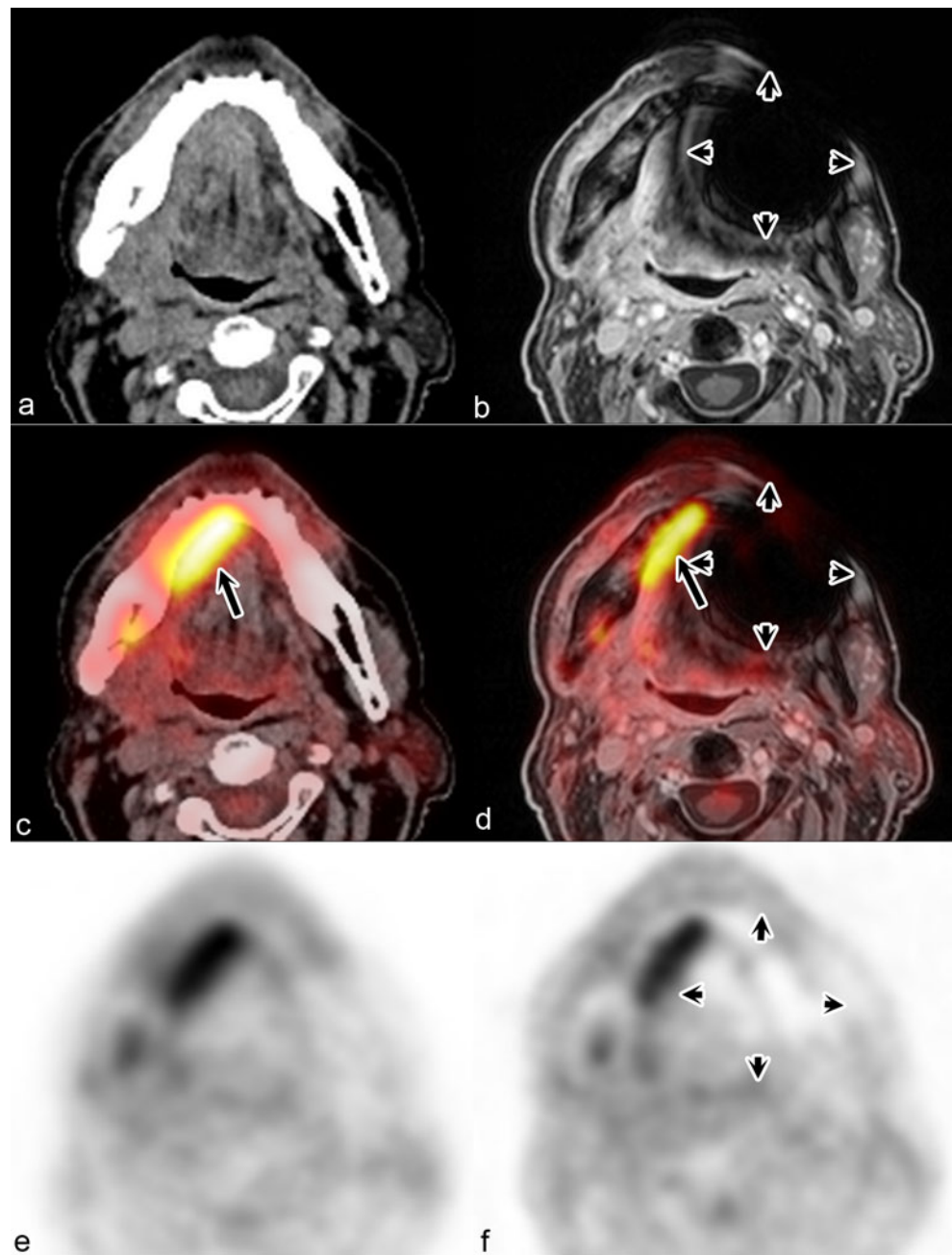

SUVs measured on PET/CT and PET/MR

SUVs were measured on PET/MR and PET/CT for the 202 lesions with focal uptake, for organs (lung, muscle, bone marrow, salivary glands, spleen and liver; 470 ROIs) and background (32; Tables 5 and 6). For malignant tumours, metastatic lymph nodes in the neck, benign lesions, bone marrow and liver, SUV_{mean} and SUV_{max} from PET/MR were significantly lower than those from PET/CT. SUV_{max} from PET/MR were also significantly lower than the corresponding values from PET/CT for the spleen and background. For all other lesions (metastatic mediastinal lymph nodes and distant metastases) and for all other organs (muscle, lung, salivary glands) there was no statistically significant difference in SUVs between the modalities.

Correlation and concordance analysis of SUVs

Spearman's correlation analysis of tracer uptake between PET/MR and PET/CT demonstrated a strong correlation for malignant uptake (SUV_{mean} $\rho = 0.877$, $n = 66$, $p < 0.001$; SUV_{max} $\rho = 0.873$, $n = 66$, $p < 0.001$), benign lesions (SUV_{mean} $\rho = 0.817$, $n = 136$, $p < 0.001$; SUV_{max} $\rho = 0.787$, $n = 136$, $p < 0.001$) and organs (SUV_{mean} $\rho = 0.868$; $n = 470$;

Fig. 3 Degraded PET/CT image quality due to dental fillings in a 73-year-old man with radiation therapy for a squamous cell carcinoma T3N2M0 of the oral cavity. **a** CT image, **b** water-only Dixon sequence image, **c** fused PET and CT image, **d** fused PET and water-only Dixon MR image, **e** PET image from PET/CT, **f** PET image from PET/MR. The PET/CT image quality is poor (score 1), but the PET/MR image quality is good (score 3). A lesion with focal uptake cannot be excluded on the PET/CT images. PET/MR data were interpreted as negative for focal uptake. The quality of PET/CT and PET/MR image fusion was comparable (score 3), (*arrows* dental artefacts)
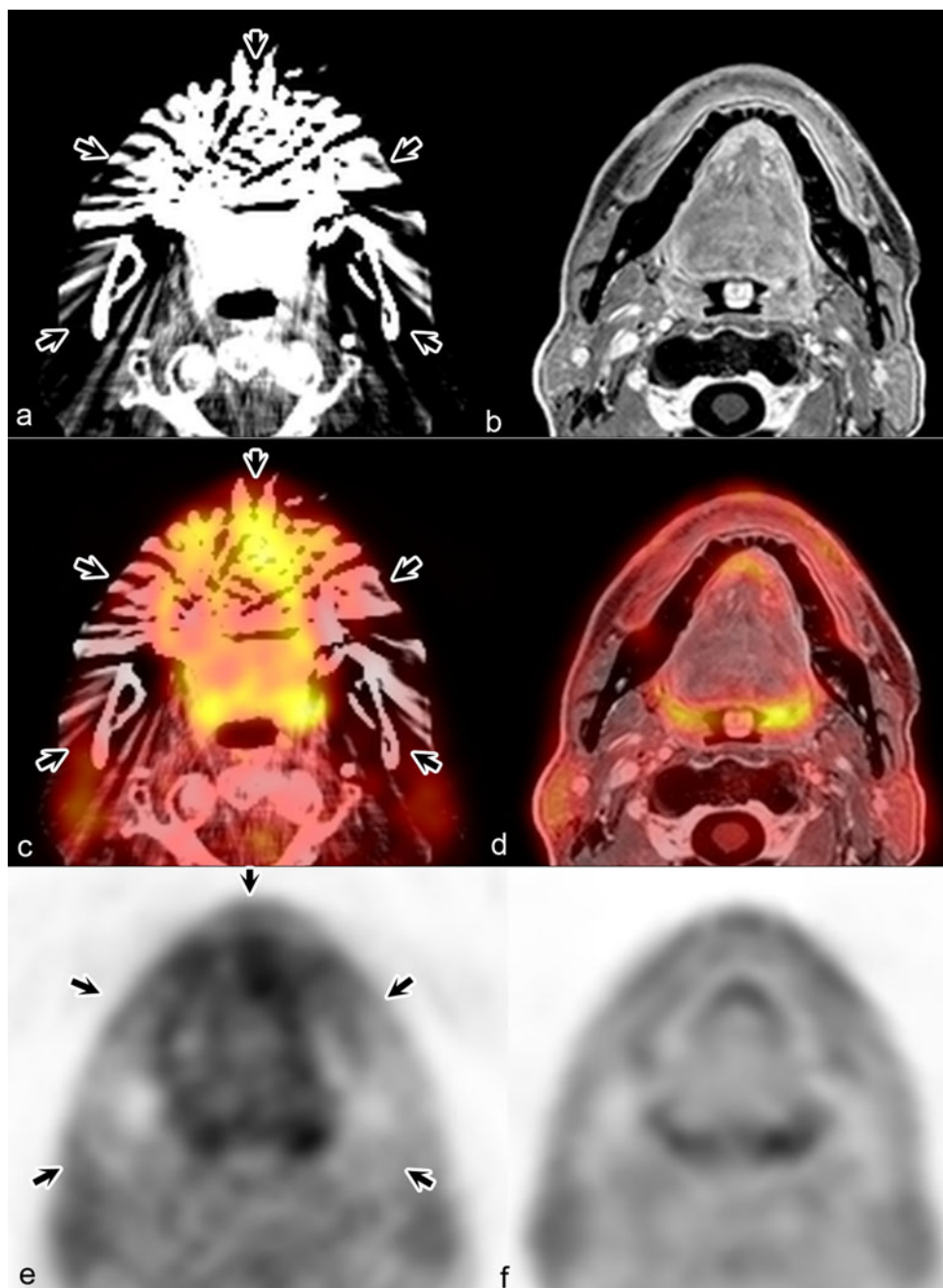
$p < 0.001$; SUV_{max} $\rho = 0.872$; $n = 470$; $p < 0.001$), as shown in Figs. 6 and 7. Bland-Altman concordance analysis for SUV_{mean} and SUV_{max} from PET/MR and PET/CT (Figs. 6 and 7) showed a systematic bias (average difference) of 3 % to 19 % of the average SUVs between organs and lesions with focal uptake. The systematic underestimation of SUVs from PET/MR compared to those from PET/CT was proportional to average SUVs. This effect was more pronounced for focal uptake than for organs. For average $SUV_{mean} > 10$ and $SUV_{max} > 12$, the relative difference in measurements was substantial (Fig. 7). Average $SUV_{mean} > 10$ and $SUV_{max} > 12$

were found in tumours with a mean size of 3.1 cm and 3.0 cm, respectively, whereas $SUV_{mean} \leq 10$ and $SUV_{max} \leq 12$ were both seen in tumours with a mean size of 1.86 cm ($p = 0.007$ and $p = 0.009$).

Factors influencing SUVs of malignant lesions

Among the tested factors (lesion size, lesion type and anatomic location), lesion size (≥ 1 cm) and lesion type were significantly correlated with SUV from PET/MR and from PET/CT ($p = 0.003$). The influence of the anatomic region was weaker

Table 2 Anatomic distribution, type and size of lesions with focal uptake

	No. (%) of lesions
Anatomic region	
Abdomen	4 (2.0)
Brain	1 (0.5)
Chest	58 (28.7)
Head and neck	139 (68.8)
Lesion type	
Malignant tumour	32 (15.8)
Malignant lymph node	23 (11.5)
Metastasis	11 (5.4)
Benign focal uptake	136 (67.3)
Lesion size (cm)[a]	
<1	53 (26.2)
≥1	149 (73.8)

[a] Maximum length according to RECIST criteria

on PET/MR ($p = 0.03$) and was nonsignificant on PET/CT ($p > 0.05$). There were significant correlations between lesion size and both SUV_{mean} and SUV_{max} from PET/MR and from PET/CT (ρ values 0.55 to 0.75, $p < 0.001$).

Factors influencing the difference between SUVs measured on PET/MR and those measured on PET/CT in malignant lesions

Anatomic region and lesion type were not associated with differences between SUVs from PET/CT and those from PET/MR ($p > 0.05$). In contrast, the size of the malignant

Table 3 Number and characteristics of benign lesions with focal uptake

	No. of lesions
Inflammation and trauma	
Reactive lymph nodes	60
Radiation-induced mucositis	19
Sialadenitis	8
Benign bone fracture	7
Oesophagitis	4
Atheromatous plaques	2
Arthritis and joint prosthesis	2
Thyroiditis	1
Pneumonia	8
Total	111
Functional hypermetabolism	
Muscle	17
Brown fat	6
Bowel motility	1
Thymus gland	1
Total	25

lesion was significantly associated with differences between SUVs from PET/MR and those from PET/CT (SUV_{mean} and SUV_{max}, $p < 0.01$). For malignant lesions <1 cm, the SUV_{mean} and SUV_{max} mean ratios for PET/MR and PET/CT were 0.97 [0.81;1.34] and 0.89 [0.72;1.15], respectively. For malignant lesions ≥1 cm, the SUV_{mean} and SUV_{max} mean ratios for PET/MR and PET/CT were 0.81 [0.70;1.00] and 0.77 [0.67;0.98], respectively.

Discussion

Coregistration of PET and MR images has recently become available in the form of integrated ("simultaneous") or dual ("sequential") technical solutions, thus combining two powerful imaging modalities that are often complementary, especially in the field of head and neck oncology. PET/MR therefore holds promise to add diagnostic value or facilitate image interpretation in a variety of clinical settings. Several research groups have reported their initial observations with PET/MR coregistration on simultaneous PET/MR systems for image acquisition in patient series with a mixed spectrum of neoplastic and inflammatory pathologies in different body regions, and the results have been favourable [12, 27].

Besides the issue of correlation between anatomic coregistration obtained with PET/MR and PET/CT, the question arises as to whether PET/MR and PET/CT provide comparable quantification of ^{18}F-FDG uptake in terms of SUVs, given that the conditions for attenuation correction may differ between the two modalities and between one body region and another.

Imaging head and neck tumours is generally challenging owing to artefacts originating from breathing and swallowing, dental implants, screws and plates that may degrade image quality [11, 14, 28]. All patients included in the current study were able to sustain both examinations. Only a small proportion of PET/MR and PET/CT images were slightly degraded and comparable scores were obtained with the two modalities for image and fusion quality, lesion conspicuity and anatomic location of focal ^{18}F-FDG uptake. No statistically significant differences were found between PET/MR and PET/CT for the number of detected foci in the lesion-based and patient-based analyses indicating that coregistration with a sequential PET/MR system is consistently feasible with good results in patients with head and neck tumours and that PET/MR and PET/CT have a similar performance for lesion detection irrespective of location, lesion category, type of malignant lesion or lesion size. Discordant readings in the current series were a result of nonvisualization of a lesion on either PET/MR or PET/CT or by discrepant categorization of a lesion seen on both modalities. The lesions missed initially on one modality were, however, identified by the two readers during retrospective evaluation.

Fig. 4 Concordant evaluation for malignant and benign lesions with focal uptake by PET/CT and PET/MR in a 65-year-old man with squamous cell carcinoma of the larynx T3N0M0. **a** CT image, **b** water-only Dixon sequence image, **c** fused PET/CT image, **d** fused PET/Dixon MR image, **e** PET image from PET/CT, **f** PET image from PET/MR. A left-sided supraglottic tumour (*arrows*) has invaded the preepiglottic space. Note the bilateral benign focal uptake of the carotid bifurcation (*arrowheads*) due to arteriosclerotic plaques
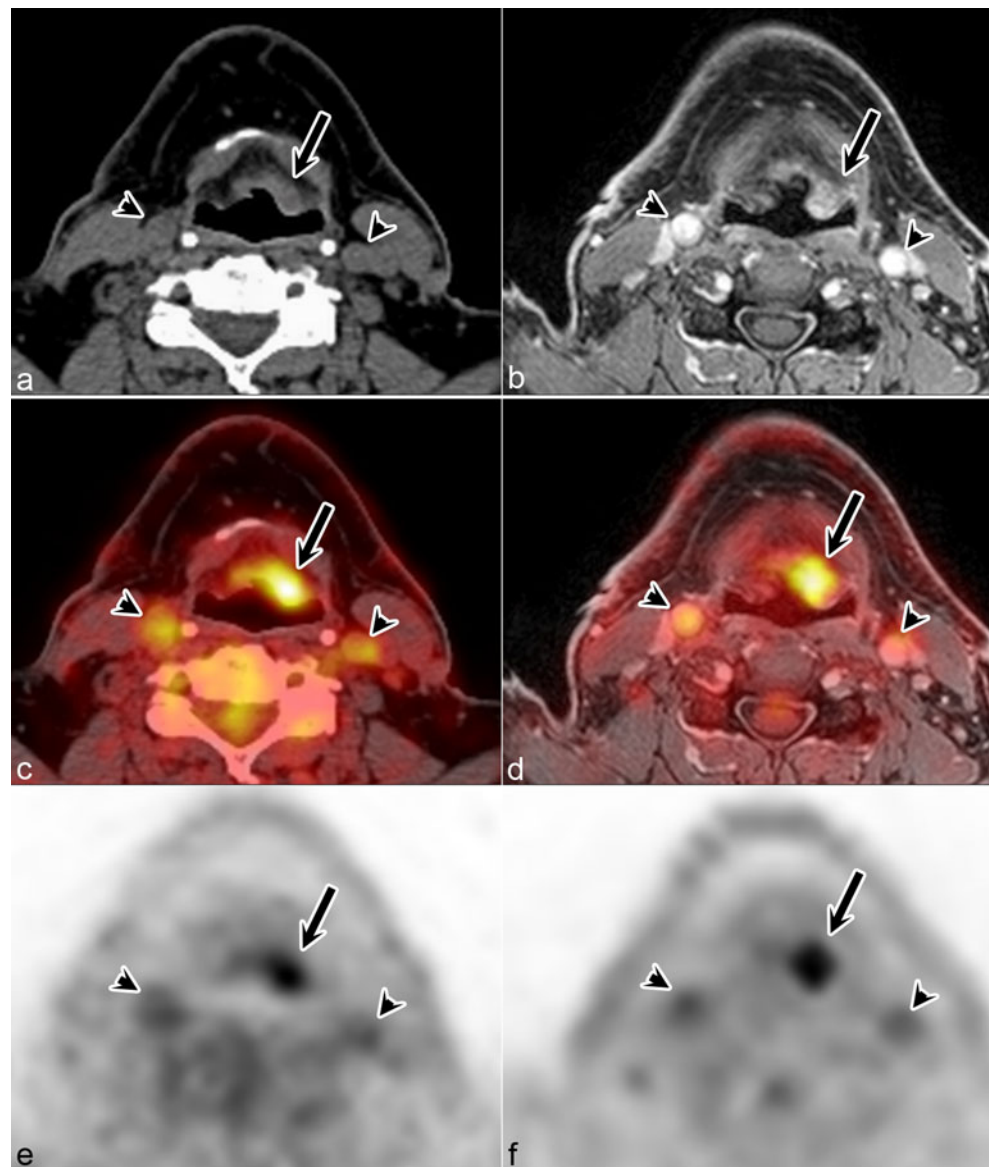

Table 4 Discordant ratings for lesions with focal uptake on PET/MR and PET/CT

Region	Type	Location	Detected on		Diagnosis on		Final diagnosis	Size[a]	SUV PET/MR		SUV PET/CT	
			PET/MR	PET/CT	PET/MR	PET/CT			SUV_{max}	SUV_{mean}	SUV_{max}	SUV_{mean}
Neck	Tumour recurrence	Maxillary sinus	No	Yes	Benign	Malignant	Inflammation	1.12	3.26	2.76	3.99	2.67
Neck	Lymph node	Level IB	No	Yes	Benign	Malignant	Inflammatory node	1.39	2.13	1.67	2.98	2.14
Chest	Lymph node	Hilum	Yes	No	Malignant	Benign	Inflammatory node	0.62	6.02	3.98	2.05	1.35
Chest	Lymph node	Hilum	Yes	No	Malignant	Benign	Inflammatory node	0.62	5.27	3.33	2.50	1.85
Chest	Metastasis	Lung	Yes	Yes	Malignant	Benign	Benign nodule	0.50	1.05	0.70	0.61	0.40
Chest	Metastasis	Bone	No	Yes	Benign	Malignant	Bone metastasis	2.05	1.38	1.18	2.65	1.74
Chest	Metastasis	Lung	No	Yes	Benign	Malignant	Inflammatory nodule	0.48	1.51	1.21	1.80	1.31
Chest	Metastasis	Pleura	Yes	Yes	Malignant	Benign	Pachypleuritis	1.44	6.44	5.00	4.68	3.59

[a] Maximum lesion length in centimetres

Fig. 5 Discordant evaluations by PET/CT and PET/MR in a 69-year-old man with histologically proven recurrent squamous cell carcinoma of the nasal cavity T2N0M0. **a**, **c** Fused PET and CT image; **b**, **d** fused PET and water-only Dixon MR image; e PET image from PET/CT; **f**) PET image from PET/MR. Evaluation of the nasal cavity tumour (**a**, **b** *arrows*) and of the right hilum and carina (**c**, **d**) is concordant. Evaluation of the left hilum is discordant (**c–f** *arrows*): PET/MR detected three lymph nodes, which were interpreted as malignant, and PET/CT detected only one node which was interpreted as malignant. Histology revealed inflammatory nodes
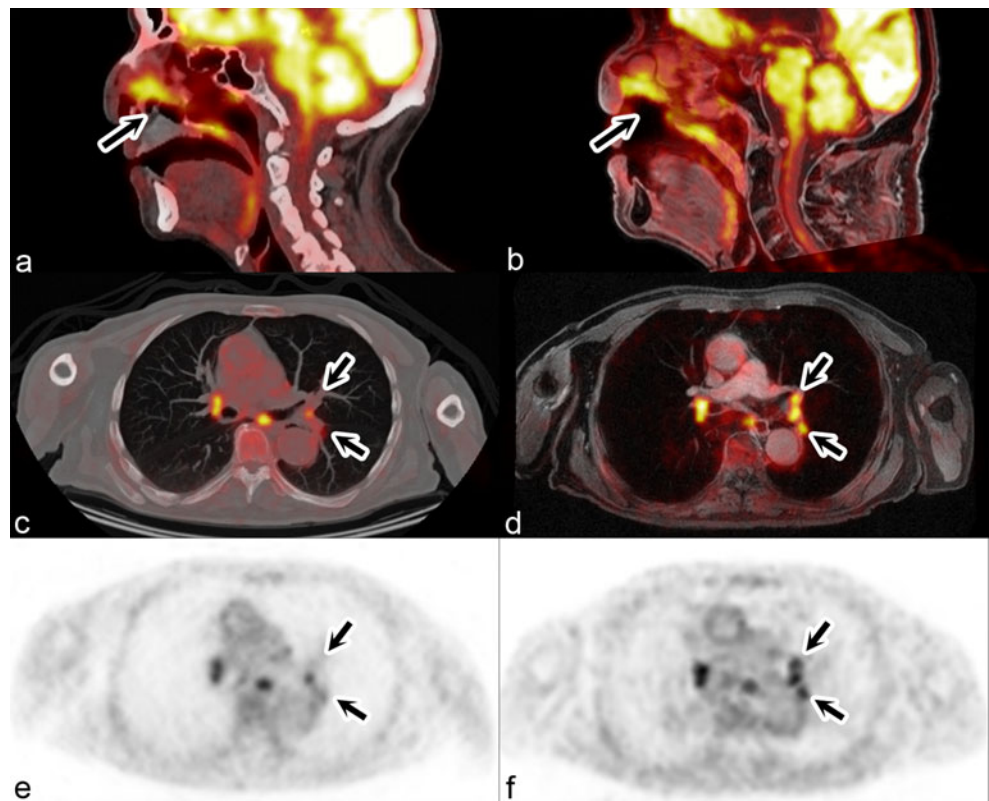
To the best of our knowledge, the accuracy of the quantitative PET information derived from sequential PET/MR in patients with head and neck tumours and the specific factors that may influence these data has not yet been determined by means of prospective quantitative analysis. PET scanner performance, data acquisition, attenuation correction method and tracer kinetics may vary among studies and may all contribute to divergent SUVs among modalities and study protocols.

The limitations of the current study comprise technical issues related to the two PET subsystems employed, the number of iterations, and the time lag between the two PET acquisitions. Technical differences between the two PET subsystems included detector design (barrel vs. pixelated Anger-logic detector), data acquisition (TF versus non-TF), and reconstruction strategies (listmode 3-D LOR–TF blob-based OSEM versus FORE+2-D AW-OSEM). We did not attempt to match the number of iterations between the two PET datasets, as matching the number of iterations will not produce images with the same quality or quantitative potential rendering evaluation of data more questionable given the differences in data sampling between the two scanners and the optimal choice of the number of subsets and subiterations. The purpose of the current study was not to validate PET/MR quantification but rather to evaluate the quantitative aspects of

Table 5 SUVs for lesions with focal uptake

Lesion		No. of lesions	Size[a]	SUV$_{mean}$				SUV$_{max}$			
				PET/MR	PET/CT	Difference (%)	p value	PET/MR	PET/CT	Difference (%)	p value
Tumour		32	2.7 [1.8;3.3]	5.5 [4.2;8.7]	7.7 [5.4;11.5]	−20.7	<0.01	6.6 [5.3;10.9]	8.7 [7.3;15.1]	−24.1	<0.01
Malignant lymph node	Neck	10	1.2 [0.8;1.4]	2.6 [2.5;5.4]	3.3 [2.9;5.8]	−16.3	<0.01	3.9 [3.4;7.3]	4.7 [4.4;8.5]	−22.0	<0.01
	Mediastinum	13	1.1 [0.6;1.4]	5.4 [4.0;6.6]	4.6 [2.5;6.5]	+13.0	0.744	7.4 [5.8;11.3]	7.8 [4.0;9.2]	+7.9	0.851
Metastasis		11	1.7 [1.4;2.1]	2.1 [1.3;2.6]	3.0 [1.9;3.4]	−12.1	0.43	2.3 [1.6;3.5]	3.7 [2.9;4.4]	−17.0	0.34
Benign focal uptake		136	1.2 [0.9;1.8]	2.1 [1.6;2.8]	2.3 [1.8;3.4]	−12.7	<0.01	2.6 [2.1;3.6]	3.2 [2.4;4.7]	−17.1	<0.01
All lesions		202	1.4 [1.0;2.1]	2.6 [1.7;3.9]	2.8 [1.9;4.5]	−13.3	<0.01	3.3 [2.3;5.3]	4.0 [2.7;6.4]	−17.4	<0.01

The data are presented as medians and interquartile intervals

[a] Maximum length in centimetres according to RECIST criteria

Table 6 SUVs for organs

Organ	No. of ROIs	SUV$_{mean}$				SUV$_{max}$			
		PET/MR	PET/CT	Difference (%)	p value	PET/MR	PET/CT	Difference (%)	p value
Lung	61	0.35 [0.30;0.42]	0.31 [0.24;0.38]	+11.0	0.03	0.43 [0.36;0.52]	0.44 [0.32;0.54]	+0.7	0.90
Muscle	182	0.78 [0.67;0.90]	0.75 [0.62;0.94]	+3.0	0.47	1.00 [0.81;1.14]	1.06 [0.86;1.30]	−4.6	0.25
Bone marrow	129	1.02 [0.59;1.41]	1.22 [0.67;1.95]	−20.0	<0.01	1.44 [0.83;1.87]	1.72 [0.96;2.51]	−20.0	<0.01
Salivary glands	37	1.57 [1.38;1.84]	1.56 [1.07;2.10]	+11.6	0.22	2.00 [1.62;2.30]	2.11 [1.74;2.75]	−4.7	0.49
Spleen	30	1.61 [1.37;1.82]	1.79 [1.46;2.02]	−7.8	0.07	2.12 [1.87;2.35]	2.43 [2.20;3.09]	−13.4	<0.01
Liver	31	1.75 [1.52;2.05]	1.99 [1.67;2.26]	−8.9	0.02	2.35 [2.00;2.68]	2.72 [2.17;3.27]	−12.7	<0.01
Background	32	1.05 [0.94;1.14]	1.11 [1.01;1.23]	−6.4	0.09	1.37 [1.22;1.50]	1.52 [1.37;1.72]	−11.9	<0.01
All	502	0.89 [0.61;1.33]	0.93 [0.59;1.49]	−4.8	0.26	1.16 [0.78;1.68]	1.30 [0.85;2.05]	−9.7	<0.01

The data are presented as medians and interquartile intervals

PET/MR compared to those of PET/CT in a clinical setting using optimized protocols for both systems, as reported recently by other investigators [12, 27]. Study logistics and timing may also play a role, as SUVs of malignant tumours may increase over time within a few hours after radiotracer injection while SUVs of inflammatory lesions tend to decrease or remain stable [29, 30]. In our study, PET/MR was performed at a mean of 61 min *prior to* PET/CT, and SUVs measured on PET/MR were significantly lower than those on PET/CT for tumours, metastatic neck nodes and benign focal
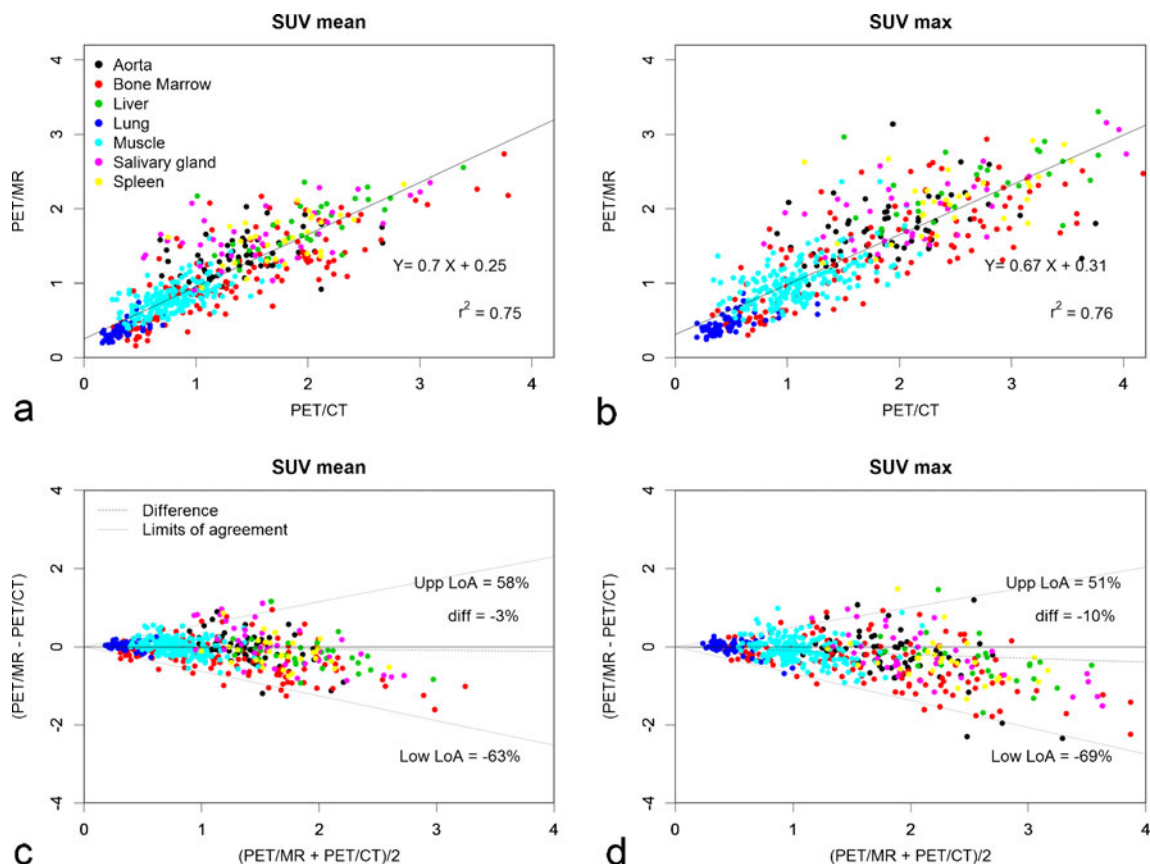
Fig. 6 Spearman correlation analysis of tracer uptake for organs (**a** SUV$_{mean}$, **b** SUV$_{max}$) shows strong positive monotonic correlations for both SUV$_{mean}$ and SUV$_{max}$ from PET/MR and those from PET/CT. SUV$_{mean}$ $\rho=0.868$, $n=470$, $p<0.001$; SUV$_{max}$ $\rho=0.872$, $n=470$, $p<0.001$. Bland-Altman plots of SUV$_{mean}$ (**c**) and SUV$_{max}$ (**d**) for organs on PET/MR and PET/CT. Differences and limits of agreement (bias±2SD) are expressed as a function of the average SUVs from PET/MR and from PET/CT. The systematic underestimation of SUVs from PET/MR is proportional to the SUV
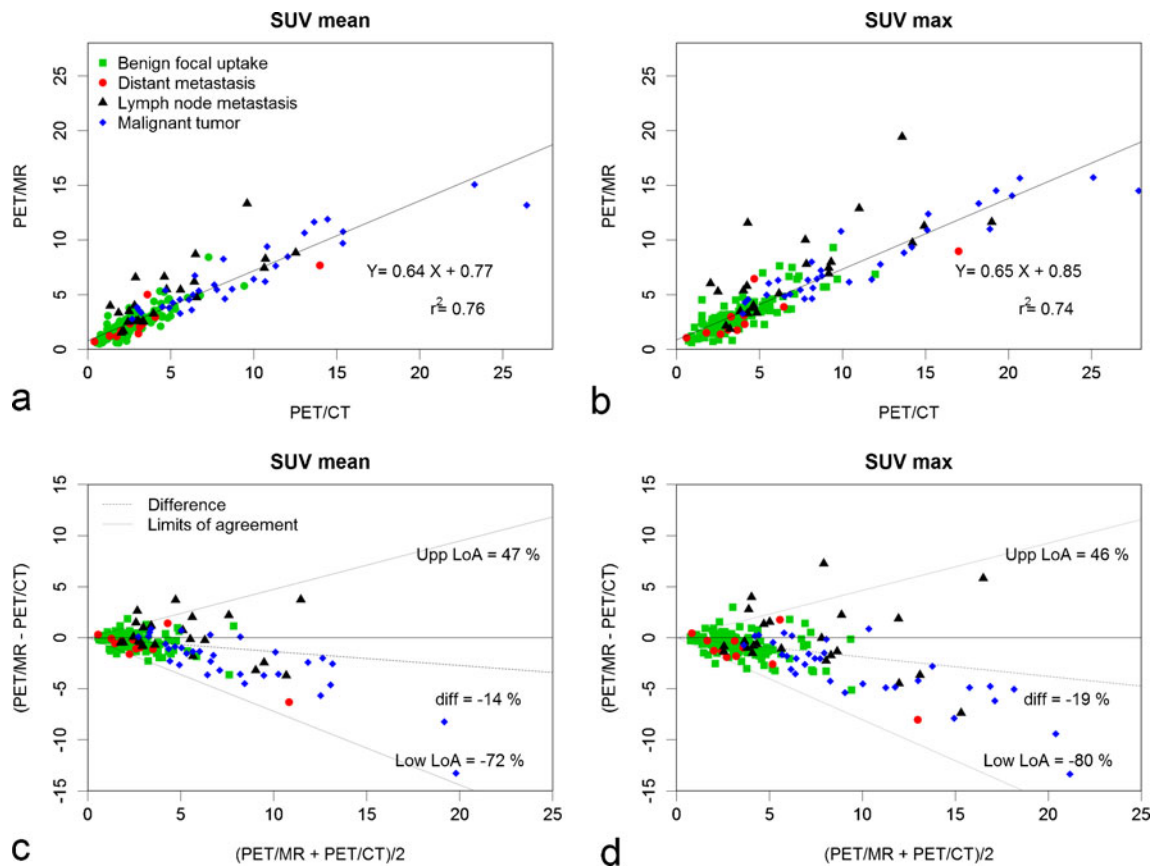
Fig. 7 Spearman correlation analysis of tracer uptake for lesions with focal uptake (tumours, metastatic lymph nodes, metastases and benign focal uptake; **a** SUV_{mean}, **b** SUV_{max}) shows strong positive monotonic correlations for both SUV_{mean} and SUV_{max} from PET/MR and those from PET/CT. SUV_{mean} $\rho = 0.872$, $n = 202$, $p < 0.001$; SUV_{max} $\rho = 0.843$, $n = 202$, $p < 0.001$. Bland-Altman plots of SUV_{mean} (**c**) and SUV_{max} (**d**) for lesions with focal uptake on PET/MR and PET/CT. Differences and limits of agreement (bias±2SD) are expressed as a function of the average SUVs from PET/MR and from PET/CT. The systematic underestimation of SUVs from PET/MR is proportional to the SUV. Note the dispersion of the data for $SUV_{mean} > 10$ and $SUV_{max} > 12$

uptake (13.3 % mean underestimation for SUV_{mean} and 17.4 % mean underestimation for SUV_{max}; Tables 5 and 6), but not for malignant mediastinal nodes or distant metastases, for which we observed only a trend. This finding can be partially attributed to the above-mentioned effect of timing, which is inherent in the design of the study, and tracer kinetics may thus have been responsible for some of the discrepant readings observed in the current study. Nevertheless, the observed underestimation of SUVs of benign lesions (mostly of inflammatory origin), as well as organs on PET/MR as compared to PET/CT (Tables 5 and 6) cannot be explained by tracer kinetics alone.

In three recent studies in which PET/MR was performed 54, 88 and 92 min *after* PET/CT, PET/MR underestimated SUVs for focal lesions and/or organs [12, 27, 31]. In two studies comparing simultaneous PET/MR and PET/CT in patients with a mixed spectrum of neoplastic and inflammatory pathologies, Drzezga et al. [12] and Wiesmüller et al. [27] found that PET/MR underestimated SUV for focal uptake in a similar range to that found in our study (11 – 12 % underestimation for SUV_{mean} and 20 % underestimation for SUV_{max}), although the two groups used different PET/MR systems, different study designs and different statistical approaches [12, 27]. From a statistical point of view, data obtained from PET scans are typically clustered data, and complicated modelling techniques may be required for correct data analysis [25, 26]. To avoid bias from multiple lesions per patient, previous investigators have used conventional statistical tests and limited their analysis to five lesions per organ or compartment [12, 27]. In our analysis, the lesions were analysed taking into consideration data clustering [25, 26]. Despite the above-mentioned differences in study design and data analysis, in accordance with previous authors [12, 27, 32] we found a statistically significant underestimation of SUVs measured on PET/MR as compared to those measured on PET/CT not only for malignant tumours and metastatic neck nodes but also for benign focal uptake, bone marrow and liver.

In agreement with previous investigators [12, 27, 32], our study also demonstrated a statistically significant strong positive correlation between SUV measurements from PET/MR

and those from PET/CT (Figs. 6 and 7) for benign and malignant lesions and for organs. However, a significant nonzero correlation coefficient does not imply that two methods are concordant [23]. Concordance of measurements obtained with two different modalities is important in terms of interchangeable use of measurements performed with either of the two modalities and in terms of facilitated comparison of quantitative data from different institutions. Quantification of tracer uptake plays an increasing relevant role in patients with head and neck cancer as an increasing number of protocols use sequential SUV measurements during treatment and in the early posttreatment phase, for the assessment of treatment response, to adapt treatment plans individually, and for systematic follow-up purposes after radio(chemo)therapy [20, 21, 33–35]. In our study, the Bland-Altman plots revealed a limited concordance of measurements in particular for lesions with high SUVs (Figs. 6 and 7). In malignant tumours, the relative difference between SUVs from PET/MR and those from PET/CT was influenced, among the factors analysed, by lesion size (the larger the tumour, the higher the SUV) and the difference in SUVs, but other factors, such as anatomic location and lesion type did not affect the difference between SUVs measured on PET/MR and those measured on PET/CT.

SUV has been shown to depend on tumour size, partial volume effect, data acquisition, reconstruction protocol and image characteristics (spatial resolution, noise, number of iterations and attenuation correction method) [36–38]. The attenuation correction method used in PET/MR ignores the presence of bony structures in contrast to that used in PET/CT. Some investigators have suggested that ignoring bone could be acceptable for the abdominal and hip regions [18, 39] but probably not in the thorax or in the head and neck [40]. Bini et al. [32] recently showed in an animal model that the MR attenuation correction method underestimated PET values by less than 10 % in most regions except areas containing bone or areas close to large bony structures. Ignoring bone might also not be adequate for quantification of osseous lesions with a reported difference between measurements on PET/MR and PET/CT of 5 – 30 % [18, 40, 41].

From a clinical point of view, our study suggests that SUVs measured on PET/MR and those measured on PET/CT may differ in particular in large head and neck tumours (Fig. 7). Although this finding may not be relevant for qualitative interpretation of PET scans for diagnostic purposes, it may have implications for tracer quantification. Therefore, when monitoring response to chemo(radio)therapy and for follow-up purposes in patients with head and neck oncology, if the initial examination was a PET/MR scan, particular care should be taken to perform the follow-up examinations on the same PET/MR machine in order to allow better evaluation of quantitative changes in tracer uptake, and vice-versa, the information that SUVs of head and neck tumours may be underestimated by 20 % using PET/MR as compared to

PETR/CT may be important for the every-day clinical use of this new hybrid technology.

Conclusion

In this study, we showed that in patients with head and neck oncology, the PET data obtained with a sequential PET/MR show equivalent findings to the PET data from PET/CT regarding image and fusion quality, lesion conspicuity, anatomic location of focal uptake, number of detected malignant and benign lesions and number of diagnosed patients with and without malignant lesions. Comparison of SUVs revealed an excellent correlation for measurements on both modalities, but underestimation of ^{18}F-FDG uptake for focal lesions (benign and malignant) and organs as compared to that estimated from PET/CT. Among the tested factors, tumour size was the major factor affecting the difference between SUV measured on PET/MR and those measured on PET/CT.

References

1. Argiris A, Karamouzis MV, Raben D, Ferris RL. Head and neck cancer. Lancet. 2008;371(9625):1695–709.
2. Becker M, Zbären P, Casselman JW, Kohler R, Dulguerov P, Becker CD. Neoplastic invasion of laryngeal cartilage: reassessment of criteria for diagnosis at MR imaging. Radiology. 2008;249(2):551–9.
3. Hustinx R, Lucignani G. PET/CT in head and neck cancer: an update. Eur J Nucl Med Mol Imaging. 2010;37(3):645–51.
4. Chawla SC, Federman N, Zhang D, Nagata K, Nuthakki S, McNitt-Gray M, et al. Estimated cumulative radiation dose from PET/CT in children with malignancies: a 5-year retrospective review. Pediatr Radiol. 2010;40(5):681–6.
5. Pichler BJ, Judenhofer MS, Catana C, Walton JH, Kneilling M, Nutt RE, et al. Performance test of an LSO-APD detector in a 7-T MRI scanner for simultaneous PET/MRI. J Nucl Med. 2006;47(4):639–47.

6. Zaidi H, Ojha N, Morich M, Griesmer J, Hu Z, Maniawski P, et al. Design and performance evaluation of a whole-body Ingenuity TF PET-MRI system. Phys Med Biol. 2011;56(10):3091–106.

7. Zaidi H, Del Guerra A. An outlook on future design of hybrid PET/MRI systems. Med Phys. 2011;38(10):5667–89.

8. Boss A, Bisdas S, Kolb A, Hofmann M, Ernemann U, Claussen CD, et al. Hybrid PET/MRI of intracranial masses: initial experiences and comparison to PET/CT. J Nucl Med. 2010;51(8):1198–205.

9. Boss A, Stegger L, Bisdas S, Kolb A, Schwenzer N, Pfister M, et al. Feasibility of simultaneous PET/MR imaging in the head and upper neck area. Eur Radiol. 2011;21(7):1439–46.

10. Schlemmer H-PW, Pichler BJ, Schmand M, Burbar Z, Michel C, Ladebeck R, et al. Simultaneous MR/PET imaging of the human brain: feasibility study. Radiology. 2008;248(3):1028–35.

11. Vargas MI, Becker M, Garibotto V, Heinzer S, Loubeyre P, Gariani J, et al. Approaches for the optimization of MR protocols in clinical hybrid PET/MRI studies. MAGMA. 2013;26(1):57–69

12. Drzezga A, Souvatzoglou M, Eiber M, Beer AJ, Fürst S, Martinez-Möller A, et al. First clinical experience with integrated whole-body PET/MR: comparison to PET/CT in patients with oncologic diagnoses. J Nucl Med. 2012;53(6):845–55.

13. Eiber M, Martinez-Möller A, Souvatzoglou M, Holzapfel K, Pickhard A, Löffelbein D, et al. Value of a Dixon-based MR/PET attenuation correction sequence for the localization and evaluation of PET-positive lesions. Eur J Nucl Med Mol Imaging. 2011;38(9):1691–701.

14. Eiber M, Souvatzoglou M, Pickhard A, Loeffelbein DJ, Knopf A, Holzapfel K, et al. Simulation of a MR-PET protocol for staging of head-and-neck cancer including Dixon MR for attenuation correction. Eur J Radiol. 2012;81(10):2658–65.

15. Delso G, Fürst S, Jakoby B, Ladebeck R, Ganter C, Nekolla SG, et al. Performance measurements of the Siemens mMR integrated whole-body PET/MR scanner. J Nucl Med. 2011;52(12):1914–22.

16. Kalemis A, Delattre BMA, Heinzer S. Sequential whole-body PET/MR scanner: concept, clinical use, and optimisation after two years in the clinic. The manufacturer's perspective. MAGMA. 2013;26(1):5–23.

17. Ma J. Dixon techniques for water and fat imaging. J Magn Reson Imaging. 2008;28(3):543–58.

18. Schulz V, Torres-Espallardo I, Renisch S, Hu Z, Ojha N, Börnert P, et al. Automatic, three-segment, MR-based attenuation correction for whole-body PET/MR data. Eur J Nucl Med Mol Imaging. 2011;38(1):138–52.

19. Huang SC. Anatomy of SUV. Standardized uptake value. Nucl Med Biol. 2000;27(7):643–6.

20. Murakami R, Uozumi H, Hirai T, Nishimura R, Shiraishi S, Ota K, et al. Impact of FDG-PET/CT imaging on nodal staging for head-and-neck squamous cell carcinoma. Int J Radiat Oncol Biol Phys. 2007;68(2):377–82.

21. Kim SY, Lee S, Nam SY, Im KC, Kim J-S, Oh SJ, et al. The feasibility of 18F-FDG PET scans 1 month after completing radiotherapy of squamous cell carcinoma of the head and neck. J Nucl Med. 2007;48(3):373–8.

22. Varoquaux A, Rager O, Lovblad K-O, Masterson K, Dulguerov P, Ratib O, et al. Functional imaging of head and neck squamous cell carcinoma with diffusion-weighted MRI and FDG PET/CT: quantitative analysis of ADC and SUV. Eur J Nucl Med Mol Imaging. 2013;40(6):842–52.

23. Kwiecien R, Kopp-Schneider A, Blettner M. Concordance analysis: part 16 of a series on evaluation of scientific publications. Dtsch Arztebl Int. 2011;108(30):515–21.

24. Bland JM, Altman DG. Measuring agreement in method comparison studies. Stat Methods Med Res. 1999;8(2):135–60.

25. Gönen M, Panageas KS, Larson SM. Statistical issues in analysis of diagnostic imaging experiments with multiple observations per patient. Radiology. 2001;221(3):763–7.

26. Galbraith S, Daniel JA, Vissel B. A study of clustered data and approaches to its analysis. J Neurosci. 2010;30(32):10601–8.

27. Wiesmüller M, Quick HH, Navalpakkam B, Lell MM, Uder M, Ritt P, et al. Comparison of lesion detection and quantitation of tracer uptake between PET from a simultaneously acquiring whole-body PET/MR hybrid scanner and PET from PET/CT. Eur J Nucl Med Mol Imaging. 2013;40(1):12–21.

28. Platzek I, Beuthien-Baumann B, Schneider M, Gudziol V, Langner J, Schramm G, et al. PET/MRI in head and neck cancer: initial experience. Eur J Nucl Med Mol Imaging. 2013;40(1):6–11.

29. Matthies A, Hickeson M, Cuchiara A, Alavi A. Dual time point 18F-FDG PET for the evaluation of pulmonary nodules. J Nucl Med. 2002;43(7):871–5.

30. Zhuang H, Pourdehnad M, Lambright ES, Yamamoto AJ, Lanuti M, Li P, et al. Dual time point 18F-FDG PET imaging for differentiating malignant from inflammatory processes. J Nucl Med. 2001;42(9):1412–7.

31. Heusch P, Buchbender C, Beiderwellen K, Nensa F, Hartung-Knemeyer V, Lauenstein TC, et al. Standardized uptake values for [18F] FDG in normal organ tissues: comparison of whole-body PET/CT and PET/MRI. Eur J Radiol. 2013;82(5):870–6.

32. Bini J, Izquierdo-Garcia D, Mateo J, Machac J, Narula J, Fuster V, et al. Preclinical evaluation of MR attenuation correction versus CT attenuation correction on a sequential whole-body MR/PET scanner. Invest Radiol. 2013;48(5):313–22.

33. Ul-Hassan F, Simo R, Guerrero-Urbano T, Oakley R, Jeannon JP, Cook GJ. Can (18)F-FDG PET/CT reliably assess response to primary treatment of head and neck cancer? Clin Nucl Med. 2013;38(4):263–5.

34. Hoang JK, Das SK, Choudhury KR, Yoo DS, Brizel DM. Using FDG-PET to measure early treatment response in head and neck squamous cell carcinoma: quantifying intrinsic variability in order to understand treatment-induced change. AJNR Am J Neuroradiol. 2013;34(7):1428–33.

35. Powell C, Schmidt M, Borri M, Koh DM, Partridge M, Riddell A, et al. Changes in functional imaging parameters following induction chemotherapy have important implications for individualized patient-based treatment regimens for advanced head and neck cancer. Radiother Oncol. 2013;106(1):112–7.

36. Hickeson M, Yun M, Matthies A, Zhuang H, Adam L-E, Lacorte L, et al. Use of a corrected standardized uptake value based on the lesion size on CT permits accurate characterization of lung nodules on FDG-PET. Eur J Nucl Med Mol Imaging. 2002;29(12):1639–47.

37. Adams MC, Turkington TG, Wilson JM, Wong TZ. A systematic review of the factors affecting accuracy of SUV measurements. AJR Am J Roentgenol. 2010;195(2):310–20.

38. Boellaard R, Krak NC, Hoekstra OS, Lammertsma AA. Effects of noise, image resolution, and ROI definition on the accuracy of standard uptake values: a simulation study. J Nucl Med. 2004;45(9):1519–27.

39. Martinez-Möller A, Souvatzoglou M, Delso G, Bundschuh RA, Chefd'hotel C, Ziegler SI, et al. Tissue classification as a potential approach for attenuation correction in whole-body PET/MRI: evaluation with PET/CT data. J Nucl Med. 2009;50(4):520–6.

40. Berker Y, Franke J, Salomon A, Palmowski M, Donker H, Temur Y, et al. MRI-based attenuation correction for hybrid PET/MRI systems: a 4-class tissue segmentation technique using a combined ultrashort-echo-time/Dixon MRI sequence. J Nucl Med. 2012;53(5):796–804.

41. Akbarzadeh A, Ay MR, Ahmadian A, Riahi Alam N, Zaidi H. MRI-guided attenuation correction in whole-body PET/MR: assessment of the effect of bone attenuation. Ann Nucl Med. 2013;27(2):152–62.